

# Generating and applying triangulations to Delaunay surfaces and combinatorial Ricci flows

Alex Henniges  
Thomas Williams  
Mitch Wilson

University of Arizona Undergraduate Research Program  
Supervisor: Dr. David Glickenstein

August 12, 2008

# Table of Contents

<b>1</b>	<b>Introduction</b>	<b>3</b>
<b>2</b>	<b>Triangulations</b>	<b>3</b>
2.1	Basics and Definitions . . . . .	4
2.2	Bistellar moves . . . . .	6
2.3	Programming Structure . . . . .	7
<b>3</b>	<b>Delaunay triangulations</b>	<b>8</b>
3.1	Definitions . . . . .	8
<b>4</b>	<b>Combinatorial Ricci flow</b>	<b>15</b>
4.1	Circle-packing . . . . .	17
4.2	Definitions and Equations . . . . .	18
4.3	Programming Ricci flow . . . . .	21
4.4	Initial testing and results . . . . .	23
4.4.1	First tests . . . . .	24
4.4.2	Morphs and specific cases . . . . .	25
4.4.3	Convergence speeds . . . . .	30
<b>5</b>	<b>Spherical and hyperbolic Ricci flow</b>	<b>33</b>
5.1	Spherical flow . . . . .	33
5.2	Hyperbolic flow . . . . .	37
5.3	Comparison of Systems . . . . .	39
<b>6</b>	<b>Future work</b>	<b>42</b>
6.1	Linking Delaunay to Ricci flow . . . . .	42
6.2	Circle packing expansions . . . . .	42
6.3	3-Dimensional triangulations . . . . .	42
<b>7</b>	<b>Conclusion</b>	<b>43</b>
<b>8</b>	<b>Appendix</b>	<b>46</b>
8.1	Derivation of Eq. (8) . . . . .	46
8.2	Proof of Proposition 3.1 . . . . .	47
8.3	Remarks on Runge-Kutta method for solving Eq. (10) . . . . .	48
8.4	Data Plots . . . . .	48
8.5	Code Examples . . . . .	51

# 1 Introduction

The purpose of this paper is to explore and extend upon the use of triangulations in Delaunay surfaces and combinatorial Ricci flow. These concepts will be addressed under an analytical structure by designing a system to represent the triangulations and provide meaningful data. A large collection of data has not yet been compiled on these concepts and our goal is for such data to solidify as well produce theories in this fairly unexplored area of mathematics. The program used for this purpose will be written in C++.

This paper will begin in §2 with an introduction to triangulations and any related definitions. Also, it will explain how our program is structured to meet its function. We will then present our research on Delaunay surfaces. That will be followed by an explanation of combinatorial Ricci flow along with the results from our initial experiments. In §5 we continue the exploration of Ricci flow under different geometries. Lastly, we will provide areas of future work on this subject.

# 2 Triangulations

Suppose you are asked to construct the surface of a sphere with as few pieces as possible. You could make a number of possible shapes, such as a cube or a soccer ball. While both of these shapes are discrete in nature, they can be used to approximate a round, continuous sphere. The most basic Euclidean approximation of the surface of a sphere is the boundary of a tetrahedron. Using only four vertices, six edges, and four faces, the tetrahedron is able to give us a surface that represents the surface of a sphere. Naturally, if we add more vertices, we are able to better illustrate our shapes through greater refinement. Similarly, in modern video games and Hollywood movies, various shapes are generated using polygons of many different sizes that mold to form a graphically rendered object. For these and all shapes, we will focus on representing them solely out of triangles. Since any regular polygon can be broken up into triangles, we can essentially represent any surface using this method.

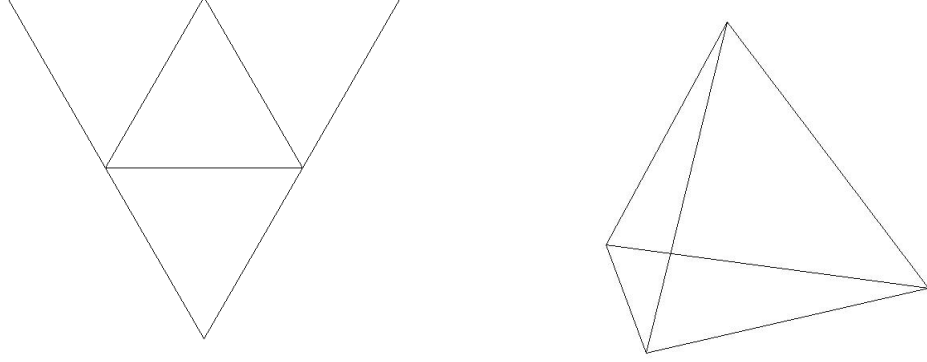


Figure 1: An example of a triangulation. In this case, the triangle, a 2-simplex, can be folded up into the boundary of a tetrahedron, a 3-simplex.

## 2.1 Basics and Definitions

For an  $n$ -dimensional space, a triangulation, written  $\tau = \{\tau_0, \tau_1, \dots, \tau_n\}$ , consists of lists of simplices  $\sigma^k$ , where the super-script denotes the dimension of the simplex and  $\tau_k$  is the list of all  $k$ -dimensional simplices  $\sigma^k = \{i_0, \dots, i_k\}$  [4]. We shall refer to 0-dimensional simplices as vertices, 1-dimensional simplices as edges, and 2-dimensional simplices as triangles or faces.

In order to describe our surfaces we must make a definition for each individual simplex. For our data structure, we decided on creating a list of references for each simplex to give it definition within the triangulation. These lists of references for each simplex are references to other simplices in the triangulation with the property of being local. We define the term “local” slightly different for each simplex. To begin with, we say that an edge is defined by two vertices and a face is defined by three vertices and three edges. Then, we can say that a vertex is local to any edge that it is in the definition of and any face that it is in the definition of, as well as any vertex that it shares an edge in common with. We say that a vertex has a *degree* equal to the number of its local edge. An edge is local to any vertex that it is defined by and any face that it is in the definition of, as well as any edge that it shares a vertex in common with. A face is local to any vertex it is defined by, any edge that it is defined by, and any face that it shares an edge in common with. These are the definitions for locality of simplices that we decided upon, creating

three different lists for each simplex.

As well as lists of references to other simplices, each simplex also has other information needed to form a triangulation. While we say that these lists of references define the topology of a given triangulation, we must provide dimensions in order to define its geometry. Namely, each edge  $\{i, j\}$  is given a length  $l_{ij}$  and each vertex  $i$  is given what we call a *weight*, denoted by  $r_i$ . We think of the weight of a given vertex to be the radius of a circle centered at that vertex. We are then able to state that for any  $n$ -dimensional simplex, there exists an  $(n - 1)$ -dimensional sphere that is orthogonal to each of the spheres centered at the vertices which define that particular simplex[4]. We use this sphere, and its center, to define the center of the given simplex. For our project, this means that a triangle  $\{i, j, k\}$  has a center defined by the center of the circle which lies orthogonally to all of the circles at each vertex, also known as the orthocircle. Additionally, each edge also has a center defined by the weights and the length of the edge.

Based on these centers, we are able to define the *local lengths* of an edge, as well as the *dual* of a given simplex, a concept that will become more important later on. For an edge  $\{i, j\}$ , it is true that

$$l_{ij} = d_{ij} + d_{ji},$$

where  $d_{ij}$  is the local length of edge  $\{i, j\}$  from vertex  $i$ , or the length from vertex  $i$  to  $C(\{i, j\})$ , the center of  $\{i, j\}$ . If we examine the edge lengths of a given triangle, it can be concluded that

$$d_{ij} = \frac{l_{ij}^2 + r_i^2 - r_j^2}{2l_{ij}} \quad (1)$$

It also holds that

$$d_{ij}^2 + d_{jk}^2 + d_{ki}^2 = d_{ji}^2 + d_{kj}^2 + d_{ik}^2 \quad (2)$$

for any face  $\{i, j, k\}$ . Based on this condition, we are guaranteed that for every face  $\{i, j, k\}$ , the perpendiculars from each edge center meet at a single point, which is the center of the face  $C(\{i, j, k\})$  as defined above[4].

There are two notable examples of choices of weights and their corresponding face centers. The first is when all of the weights are zero. In this case, a

triangle center  $C(\{i, j, k\})$  is the center of the circumcircle of  $\{i, j, k\}$ . The second is when the weights are equal to the local lengths for  $i$ , or for all vertices  $j$  and  $k$  that are local to  $i$ , we have  $d_{ij} = d_{ik}$ . This case is known as a *circle packing* and will be used in the material discussed in §4. In this case, a triangle center  $C(\{i, j, k\})$  is the center of the incircle of  $\{i, j, k\}$ .

We will now make definitions for duals of our simplices. First, the dual of a face is simply its center  $C(\{i, j, k\})$  as defined above. Now we will define a dual for a given edge. Let us refer to any edge, along with the faces of which it forms an intersection, as a *hinge*. We are able to embed any hinge in the plane. Because of (2), we know that on any hinge in the plane, the center of an edge along with the centers of its two local faces are colinear. The line connecting these three points is the dual for the given edge. We can determine the length of this dual if we can determine the length of the line segment connecting the center of an edge to the center of one of its local faces. On triangle  $\{i, j, k\}$ , we can write the distance between  $C(\{i, j\})$  and  $C(\{i, j, k\})$  as

$$d[C(\{i, j\}), C(\{i, j, k\})] = \frac{d_{ik} - d_{ij} \cos(\theta_i)}{\sin(\theta_i)} \quad (3)$$

where  $\theta_i$  is the angle at  $i$  on face  $\{i, j, k\}$ . In the case that  $C(\{i, j, k\})$  lies outside of  $\{i, j, k\}$ , then this distance has a negative value. Otherwise, the distance is positive[4]. Naturally, the dual of a given edge has a distance that is obtained by adding the distances from the center of the edge to the centers of each face it is local to. The dual of a given vertex  $i$  is the area enclosed by the duals of every edge local to  $i$ . The duals of edges will be talked about again in 3.

## 2.2 Bistellar moves

On a given triangulation, we are able to perform different modifications, which we will refer to as *bistellar moves* or *flips*. There are three possible bistellar moves that can be performed on a 2-dimensional triangulation: a 1-3 move, a 2-2 move, and a 3-1 move. One way to understand these moves, and where the term *flip* comes from, is to imagine holding in your hand a tetrahedron. You can look at this tetrahedron three different ways, at a face, at an edge, or at a vertex, and see a different image, as it would be embedded in the

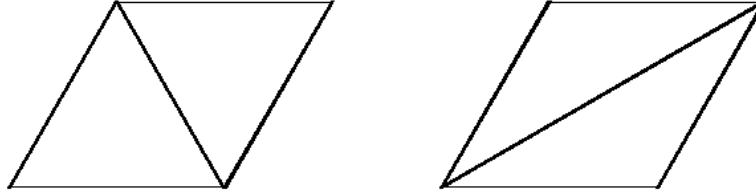


Figure 2: An example of a 2-2 flip.

plane. If you were to “flip over” this object, you would see the reverse image which would describe the 2-dimensional image resulting from what we call a *flip*. The image of a face would be replaced by the image of a face with an additional vertex in the middle of it. The image of an edge, a hinge as it were, would be replaced by the image of itself rotated  $90^\circ$ . The image of a vertex, as seen within a face, would be replaced with just a face. These moves respectively describe the 1-3, 2-2, and 3-1 moves.

We will now describe these moves in terms of a triangulation. For a 1-3 move, we take a single face and place a vertex in the middle of it. We then add three edges connecting this vertex to the existing vertices of the face. For a 2-2 move, we look at the hinge. The move consists of removing the edge that describes the hinge and replacing it with an edge that connects the opposite two vertices of the hinge. See Figure 2. For a 3-1 move, what is essentially the inverse of the 1-3 move, we look at a vertex of degree three in addition to the face defined by the three vertices it is connected to. We then remove this vertex along with the three edges local to it and we are left with just a single face.

## 2.3 Programming Structure

When creating the program, the data structure design was critical. The design not only helps dictate the direction of the project over the course of its lifespan, but the decisions affect the speed and efficiency of all added functionality. It was agreed that the system would have to hold the different simplices and that they would be referencing each other. This part of the program would need to be structured in a way that makes it quick and easy

to move from one simplex to another. As seen in Figure 3, all simplices are assumed to have lists of references to other simplices, what we call local simplices, broken down by dimension. For the two-dimensional case, each simplex has lists of local vertices, local edges, and local faces.

The lists are vectors of integers. The vector, provided in the C++ library, was chosen so that the list can dynamically change in size. The integers are a decision based on both speed and size. Instead of, for example, a vertex having a list of actual edges ( $\overline{AB}$ ,  $\overline{CF}$ , etc.) or pointers to edges, the vertex has a list of integers representing the edges. The actual edges are then obtained through the *Triangulation* class, which holds maps from integers to simplices. The *Triangulation* class is made up of static functions and maps and is designed so only one triangulation exists at any time. Because the maps are static, they can be accessed at any time from anywhere in the code without the need to pass pointers through function calls.

## 3 Delaunay triangulations

### 3.1 Definitions

One special type of triangulation is known as a *Delaunay triangulation*, of which there are two different types. The first type is the case of non-weighted triangulations, which we simply call “Delaunay”, while the second type is reserved for weighted triangulations, which we refer to as “weighted Delaunay”. Before we can define what it means for a triangulation to be Delaunay or weighted Delaunay in a global sense, we must define what it means for a triangulation to have either of these conditions in a local sense, and in order to do that, we must consider a single hinge.

To determine if a hinge is Delaunay, we must consider the orthocircle of both of the triangles in the hinge. In the non-weighted case, this is the circumcircle of the triangle. If the circumcircle of either of these triangles (and as it turns out, necessarily both of them) contains the opposite vertex contained in the hinge, then we say that the hinge is not Delaunay. However, if both triangles have circumcircles that do not contain the opposite vertex on the hinge, then the hinge is Delaunay. It is worth noting that all non-convex



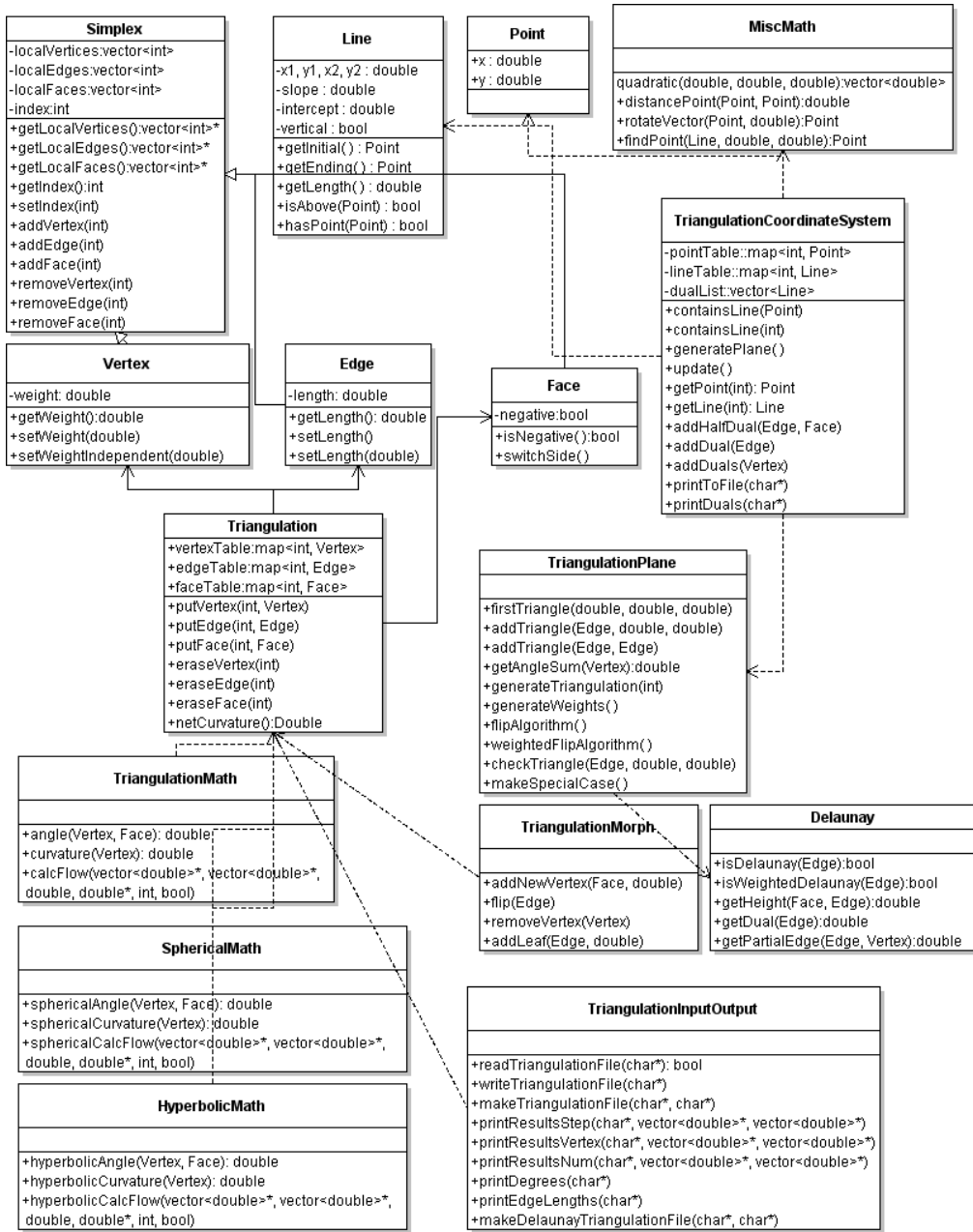


Figure 3: A UML diagram of the program. The UML shows how the various files interact as well as the functions and variables they hold. We will refer to many of these programs later on.

hinges, that is all hinges with one of the angles on the edge having a measure greater than  $\pi$ , are Delaunay.

**Proposition 3.1.** *The sum of the opposite angles on a non-Delaunay hinge is greater than  $\pi$ .*

**Corollary 3.2.** *Any non-Delaunay hinge will become Delaunay after a 2-2 flip is performed on it.*

This proof is given in 8.2. One thing that is important to note after the discovery of this property is what we refer to as the “convergent case”, the case where the hinge forms a cyclic quadrilateral, one where all the vertices lie on the same circle. This occurs when the centers of the triangles, given by the centers of their orthocircles, lie on the same point. In such a case, the hinge is considered to be Delaunay, as well as its flipped image.

The condition of a hinge being weighted Delaunay is somewhat different. As stated before the dual of a hinge is found by connecting the centers of the two orthocircles. In the case of a weighted triangulation, a hinge is weighted Delaunay when the dual has positive length. Recall that the length from the center of an edge to the center of its local face, half of the length of a hinge’s dual, is measured as negative if the center of the triangle lies outside of the triangle itself.

One result of the variance in definition between Delaunay and weighted Delaunay is that a hinge that is nonconvex can also be not weighted Delaunay. This creates issues when one wishes to perform flips on hinges that are not weighted Delaunay. It is not entirely clear, at first, how one goes about performing a flip on a hinge that is nonconvex. The picture on the left in 3.1 shows such a hinge before the flip is performed. The picture on the right shows the resulting image of a triangle with an “anti-triangle” lying over a portion of it. We consider this triangle to have negative area, its angle to have negative measure, and its half-duals to be of negative length.

There are a number of remarks to be made regarding negative triangles in our triangulations. First of all, we can give all of our triangles a score, based on their positive or negative orientation, of either 1 or -1. Using this, we can create a value for any point in the boundary of a given triangulation.

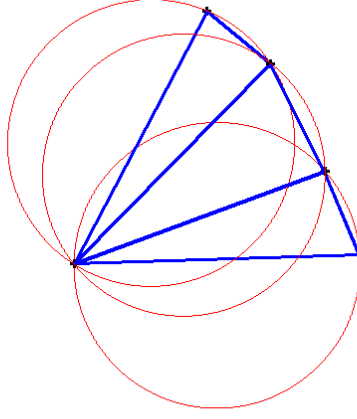


Figure 4: A simple example of a Delaunay triangulation. The circumcircles are drawn along with the edges to show their compatability. This is a non-weighted case.

Regardless of the number of flips performed, where, or how many negative triangles are created from them, if one were to pick any point within the pre-existing boundary, the value is guaranteed to be one. That is to say, for every negative triangle or set of negative triangles created, there is a positive or set of positive triangles created to completely cover them. Additionally, if there is a nonconvex hinge that lies on the border that is flipped

We can produce a non-weighted Delaunay triangulation using mathematical software like MATLAB. However, less is known about weighted triangulations in general. For this project, we aim to develop an algorithm that can create a valid triangulation, add weights to vertices, and manipulate the faces to produce a Delaunay triangulation.

An important aspect to properly explore these triangulations is in their generation. We developed a program *generateTriangulation* which can generate a determined number of faces with a random configuration. To truly test our algorithms and to provide convincing results would require an unbiased way of constructing the triangulations. There are several properties to triangulations that we wish to be randomized, and they include the lengths of each edge, the degree of each vertex, and the weight at each vertex. It is unclear

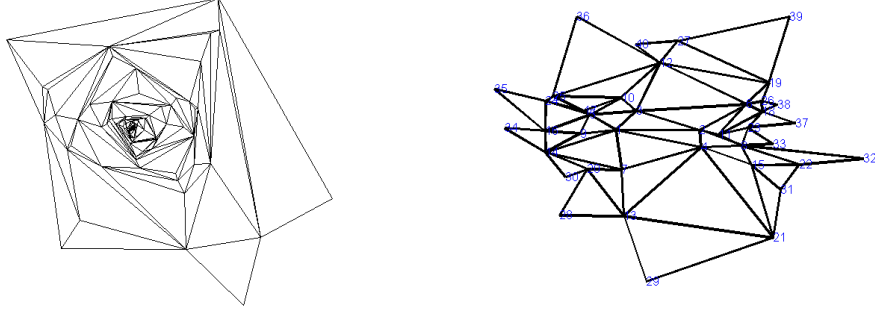


Figure 5: Two examples of triangulations using our *generateTriangulation* program, an early version (left) and a modern version (right). The early version wound up spiraling around itself, increasing edge lengths as it went. Our newer version makes the edge lengths more random, with large and small triangles scattered throughout.

if there is a way to provide a truly random generation of triangulations or even if such a system would be desirable, but we feel that the algorithm we chose adequately meets our goals.

Our random triangulation generator begins with one triangle with edge lengths between 0.0 and 10.0. This was chosen arbitrarily as all future weights will be based off of these. Triangles are then created from each edge along the border. When the creation of an edge would result in a vertex's angles summing to greater than  $2\pi$ , we instead close off the vertex by connecting its two outer edges. Once the desired number of faces have been created, the algorithm ends. Section [] in the appendix shows several results of this algorithm.

We can generate weights at random by restricting their maximum size with respect to the shortest edge length in the triangulation, so as not to make weights too large. We can also assign weights to individual vertices such that others remain unweighted.

In order for a triangulation that we have created to be Delaunay, we must be able to guarantee that all orthocircles behave as they should. However, in our generation, we may create triangles that can make the end result hard to obtain. At times, we create triangles in which the largest side length is barely

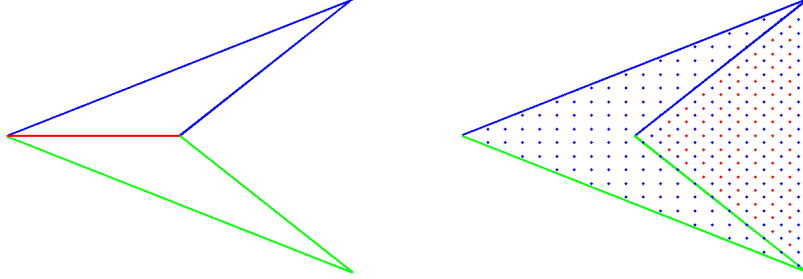


Figure 6: If flips are performed on nonconvex triangles, we create an anti-triangle, shaded here in red, and a larger regular triangle, shaded in blue.

smaller than the sum of the other two sides, or “skinny triangles.” We find that the orthocircles related to these triangles have a large tendency to make the triangulation not Delaunay as the orthocircle is very large with respect to the dimensions of the triangle, and thus they like to contain other vertices.

We feel that if a triangulation is not Delaunay, we can perform a series of 2-2 flips on various surfaces until it results in a Delaunay configuration. We do not change the vertices in any fashion or the number of triangles, only how they are connected to each other.

One issue we noted was that certain flips would change our notion of triangles. Flips sometimes produced triangles where they did not exist before. We call these anti-triangles, or *negative triangles*. See Figure 6. We can check for cases when this may happen and adapt our flipping process as needed.

The dual lengths of negative triangles are exactly opposite in length than of a congruent regular triangle. Similarly, we say that a negative triangle has a negative area in order to conserve area, as can also be seen in Fig. 6.

We created a program called *weightedFlipAlgorithm* that scans each edge to see if it was Delaunay, and if not, we would perform a flip on the two faces of which the edge is connected. We would repeat the process until (hopefully) each face was Delaunay, and thus the whole triangulation was now Delaunay. Unfortunately, the process did not always end.

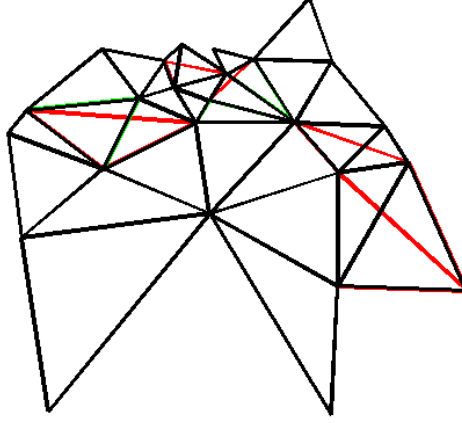


Figure 7: An illustration of our *delaunayPlot* program. The end triangulation is shown in black. Original edges that were later flipped are shown in red.

To get a better grasp of the evolution of the flips, we made a MATLAB program named *delaunayPlot* that would draw a triangulation so we could visually ensure that our triangulations were being built correctly and also if and where flips were being performed, as well as tracking negative triangles. We use MATLAB as it is able to read data from files, like in C++, as well as generate pictures relatively easily. We adapted this code to then make *multiDelaunayPlot*, which regraphs the triangulation after a flip is performed. See Figure 7 for a beginning and end triangulation after going through *weightedFlipAlgorithm*.

Often times, we did find that triangulations were able to become Delaunay after a series of flips. As we added more faces, and increased weights by scalars, we noted that it was more likely for the algorithm to have issues. See Table 1. In watching our *multiDelaunayPlot* results, we found that certain edges would loop in a series of flips such that performing one flip would require the adjacent edge to need flipping. Occasionally, one edge would get stuck flipping back and forth between two faces. We also noted that final triangulations did permit the existence of negative triangles. Often they were

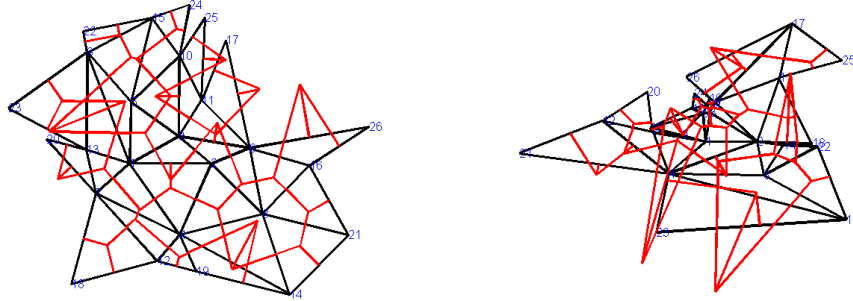


Figure 8: A non-weighted (left) and weighted (right) triangulation with dual lengths added.

found on the edge boundary and of little concern. We were able to check our results by drawing the dual edges on top of all the faces (Refer to our criteria in §2.1 and §3.1. If all vertices had zero weight, then the duals are simply the perpendicular bisectors of each edge. See Figure 8.

We also observed a couple of interesting things from a statistical point of view. We found that, after flips were performed, the average length of all edges tended to decrease by a small amount. This would lead to suggest that vertices try and form triangles with vertices close to itself, resulting in fewer skinny triangles. We also saw that the degrees of vertices tend to vary more after flips; more have a degree of 2 or 3, while others increase in degree. This suggests that the weights of vertices in its triangulation also has a great effect as well as their relative proximities. See Figure 9 for an example with a non-weighted case.

So to conclude, yeah, flips are awesome. We show that flips can be performed on ANY triangulation, not just certain ones. By using neative triangles, we are able to adapt our code for extraneous cases.

## 4 Combinatorial Ricci flow

Introduced by Richard Hamilton in 1982, Ricci flow, named in honor of Gregorio Ricci-Curbastro [6], has since had a large influence in the world of

Scalar = 1.0			Scalar = 1.5		
Faces	Avg. Flips	% Finish	Faces	Avg. Flips	% Finish
25	4.1	100	25	13.5	83.33
50	11.2	100	50	19.6	71.29
100	26.8	100	100	41.7	40

Table 1: An anlysis of number of flips required to obtain Delaunay triangulation for a given number of faces and scaled weights. Each test was performed on *weightedFlipAlgorithm* until each test had ten successful runs. Each trial had unique weights.

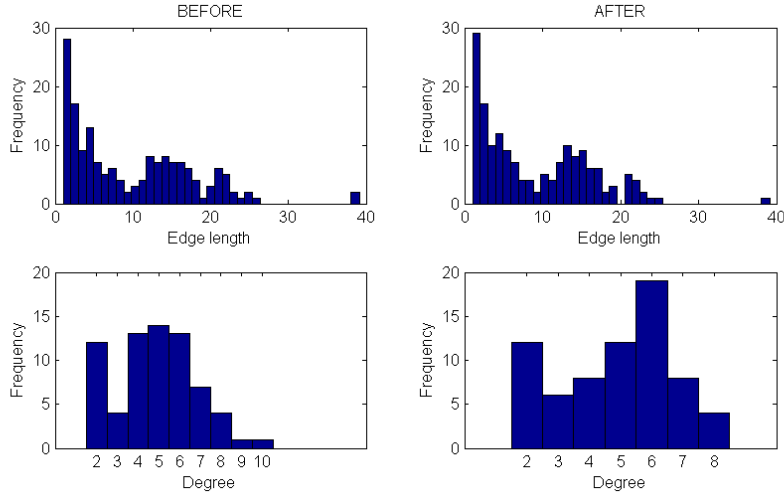


Figure 9: A statistical illustration of edge lengths and vertex degrees before and after flips are performed.



geometry and topology. It is often described as a heat equation. Imagine a room where a fireplace sits in one corner and a window is open on the other side. The heat will diffuse through the room until the temperature is the same everywhere. With Ricci flow, the same occurs with the curvature. Under Ricci flow, a geometric object that is distorted and uneven will morph and change as necessary so that all curvatures are even. The biggest consequence of Ricci flow came when Grigori Perelman proved the Poincaré Conjecture in 2002. The Poincaré Conjecture, proposed in 1904, was particularly difficult to prove, and was given the honor of one of seven millennium puzzles by the Clay Mathematics Institute. It was Ricci flow that turned out to be the cornerstone for the proof. In addition, its relation to the heat equation may open new doors for work in fluid dynamics and even in the theory of general relativity [6]. In 2002, Chow and Luo introduced the concept of combinatorial Ricci flow. They showed that this new concept, performed on a triangulation of a manifold, had many of the properties of the Ricci flow Hamilton had defined. The fact that the subject is still very new makes this research project exciting.

## 4.1 Circle-packing

Looking back at our weighted Delaunay triangulations, we had the condition that the partial edge lengths were related by Eq. (2). As mentioned in §2.1, let us take a subset of all possible weight configurations and develop further the concept of circle-packing. Visually, circle-packing entails placing circles with their centers on a vertex so that neighboring circles are tangent to each other. That is, they intersect at only one point, as shown in Figure 10. Thus, we have the restrictions that  $d_{ij} = d_{ik} = r_i$ ,  $d_{ji} = d_{jk} = r_j$ , and  $d_{ki} = d_{kj} = r_k$ , ensuring that 2 holds. For any lone triangle, this can be done. By applying weights to each vertex we determine the lengths to the edges of our triangulation as  $l_{ij} = r_i + r_j$ , where  $r_i$  and  $r_j$  are the radii of the circles centered at vertices  $v_i$  and  $v_j$ , and  $l_{ij}$  is the length of  $\{i, j\}$ . In Euclidean space, the metric applied to the triangulation in this way is known as the *cone metric* [2].

Choosing to define the metric in this way, we guarantee the triangle inequality and ensure that we are creating triangles. It is also needed to run the combinatorial Ricci flow, explained in §4.2. But, there are restrictions to ap-

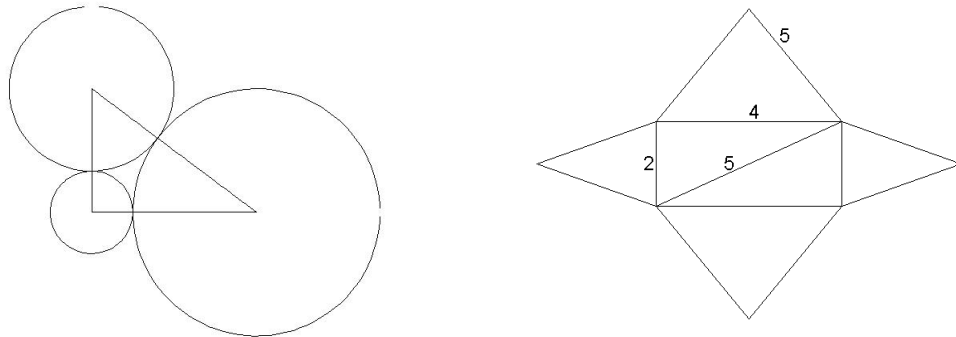


Figure 10: An example of circle packing (left) and a triangulation that cannot be circle-packed.

plying weights first. Not all combinations of edge lengths are possible under this system. Some triangulations can simply not be circle-packed. An example is shown in Figure 10, where there is no combination of weights at the vertices that can make a proper circle-packing. By allowing generalizations of circle-packings, as discussed in §6.2, we can broaden our range of possible length assignments.

## 4.2 Definitions and Equations

We define a manifold to be a topological space where every neighborhood is locally Euclidean. This means that around any point in the space it appears similar to the sphere locally. What this means for our triangulated surfaces is that there are no borders. We also refer to this as a closed triangulation.

When talking about closed, triangulated surfaces, one such important property related to the surface is known the Euler characteristic  $\chi$ , defined by the equation  $\chi = V - E + F$ , where  $V$  is the number of vertices in the triangulation,  $E$  is the number of edges, and  $F$  is the number of faces. This characteristic is directly connected to another important property, the *genus* of a surface. The genus of a surface is the topological property that is more loosely known as the number of “holes” in the surface. For instance, a sphere has a genus of 0 while a torus has a genus of 1, a two-holed torus has genus 2, etc. The relationship between the two values is given by  $\chi = 2 - 2g$ , where

Name	Vertices, V	Edges, E	Faces, F	Genus, g	$\chi$
Tetrahedron	4	6	4	0	2
Octahedron	6	12	8	0	2
Icosahedron	12	30	20	0	2
Torus	9	27	18	1	0
Two-holed torus	10	36	24	2	-2

Table 2: Listings of vertices, edges, faces, and genus for some common shapes

$g$  is the genus of the surface.

Once we have a triangulation and it is circle packed, our manifold may not be in its most compact form. We would like to have a way to determine the evolution of each shape to its final configuration, which may be more uniform. We introduce combinatorial Ricci flow to the system. On a discrete surface, this equation allows the weights to change over time [2]. We present the equation to the reader, which can be written as

$$\frac{dr_i}{dt} = -K_i r_i \quad (4)$$

where  $K_i$  is a characteristic called the *curvature* of a vertex, and  $r_i$  is the *weight* of the vertex  $i$ . The value of  $K_i$  changes with time. Its value is found by determining the angles of all triangles containing vertex  $i$ . Using side lengths we can determine the angle using the law of cosines. For a triangle with lengths  $a, b$ , and  $c$ , the angle opposite side  $c$  is

$$\angle C = \arccos\left(\frac{a^2 + b^2 - c^2}{2ab}\right)$$

with similar formulas for the other angles. We take the sum of all angles associated with a vertex  $i$  and define the curvature  $K_i$  as

$$K_i = 2\pi - \sum \angle i. \quad (5)$$

Since we are performing multiple non-linear differential equations as variables depend on the weights which change over time, we can probably not solve them explicitly.

A potential issue we noted is that, based on the equation, is it possible that the radii could continually decrease. Take, for example, a simple tetrahedron

with all sides of equal length. We find that the curvature of each vertex always equals  $\pi$ . Thus in solving the differential equation computationally we would decrease each vertex weight by the same amount, but the curvature of each vertex would still remain  $\pi$ . This is because, in the Euclidean case, the curvatures are not affected by uniform scaling. Under (4), the radii would continue to decrease until they approach zero length. We have to address that issue since computers don't like working with numbers near zero, as in the denominator of the arccosine function. Numerical instability may occur. To avoid this issue, let us resize the length of each radius by a scalar,  $\alpha$ . We denote each scaled length by  $\tilde{r}_i$  and equate as

$$\tilde{r}_i = \alpha r_i.$$

Each  $\tilde{r}_i$  would have its own  $\tilde{K}_i$ , but since we are scaling all sides by the same factor, this does not effect the curvature of the surface, so  $\tilde{K}_i = K_i$ . Thus in plugging  $\tilde{r}_i$  in to the differential equation we get

$$\begin{aligned} \frac{d\tilde{r}_i}{dt} &= \frac{d(\alpha r_i)}{dt} = \alpha \frac{dr_i}{dt} + r_i \frac{d\alpha}{dt} \\ &= -\alpha K_i r_i + \frac{\tilde{r}_i}{\alpha} \frac{d\alpha}{dt} \\ &= -\tilde{K}_i \tilde{r}_i + \frac{\tilde{r}_i}{\alpha} \frac{d\alpha}{dt}. \end{aligned} \tag{6}$$

We also note that  $\frac{1}{\alpha} \frac{d\alpha}{dt} = \frac{d(\log \alpha)}{dt}$  using a basic chain rule. In order to find an appropriate value for  $\alpha$  we decided to use the following criterium:

$$f(\tilde{r}_1, \tilde{r}_2, \dots, \tilde{r}_n) = \prod \tilde{r}_i = \prod \alpha r_i = C, \text{ a constant.} \tag{7}$$

We will call this value the *product area* of the surface. This area prevents all radii from decreasing to zero at the same time. By taking the derivative of Eq. (7) with respect to time we find that

$$\frac{d(\log \alpha)}{dt} = \frac{\text{sum of all curvatures}}{\text{number of vertices}} = \overline{K}, \text{ average curvature.} \tag{8}$$

In this paper, we may refer to the sum of all curvatures as the *total curvature*. We can also show that  $\overline{K}$  is a constant and depends on the number of vertices and the Euler characteristic. We know that the sum of angles from each

vertex is  $360^\circ$ , or  $2\pi$ . However, we also know that the sum of angles on each face is  $\pi$ , thus we determine that

$$\sum K_i = 2\pi V - \pi F = 2\pi(V - \frac{F}{2})$$

We can simplify this by noting trends in basic triangulations. As every face is made up of three edges, and each edge belongs to two faces, we can see that  $3F = 2E$ , or  $E = \frac{3F}{2}$ . Looking back at Table 2 we note this true for all polyhedra listed. Let us use this substitution and rewrite the above equation as

$$\sum K_i = 2\pi(V - \frac{F}{2}) = 2\pi(V - \frac{3F}{2} + F) = 2\pi(V - E + F) = 2\pi\chi.$$

Thus we find that  $\bar{K}$  is just  $\frac{\sum K_i}{|V|} = \frac{2\pi\chi}{|V|}$  where  $|V|$  is the number of vertices. This is also noted in [2]. Plugging this information back into Eq. (6) we determine that

$$\frac{d\tilde{r}_i}{dt} = -\tilde{K}_i\tilde{r}_i + \bar{K}\tilde{r}_i = (\bar{K} - \tilde{K}_i)\tilde{r}_i \quad (9)$$

However, since everything is now a function of  $\tilde{r}_i$  and not  $\alpha$ , we can just as easily plug  $r_i$  back in to the differential equation instead of  $\tilde{r}_i$ , so we end up with:

$$\frac{dr_i}{dt} = (\bar{K} - K_i)r_i \quad (10)$$

This is known as normalized Ricci flow, as discussed by Chow and Luo in their paper [2]. In the case of our basic tetrahedron from earlier, the radii would not change after each iteration as  $\bar{K} = K_i = \pi$  and thus  $\frac{dr_i}{dt} = 0$  for  $i = \{1, 2, 3, 4\}$ .

### 4.3 Programming Ricci flow

While we are able to create our own triangulations from scratch, we noted an odd characteristic. The value of  $\chi$  on our triangulations always equaled 1. However, for spheres and tori we know that  $\chi = 2 - 2g$ , with  $g$  being the number of “holes.” We noted that since our border edges contained unique

Vertex: 1	Edge: 1	Face: 1
2 3 4	1 2	1 2 3
1 2 4	2 3 4 5 7	1 2 3
1 2 3	1 2	2 3 4
Vertex: 2	Edge: 2	Face: 2
1 3 4 5	1 3	1 2 4
1 3 5 7	1 3 4 6 8	1 4 5
1 2 4 5	1 3	1 3 5
⋮	⋮	⋮
Vertex: 5	Edge: 9	Face: 6
2 3 4	4 5	3 4 5
7 8 9	4 5 6 7 8	6 8 9
4 5 6	5 6	3 4 5

Table 3: Conversion of format from [5] to ours.

vertices, we could not easily transform our triangulation into a common manifold.

Frank Lutz, creator of The Manifold Page [5], has a catalog of almost two million known manifold triangulations of varying sizes. However, the format is different than our setup, so we developed an algorithm to take a given triangulation, saved on its own as a text file, and convert it into the form that we use. We were able to transform this

```
{manifold_lex_d2_n5_o1_g0_#1=[[1,2,3],[1,2,4],[1,3,4],
[2,3,5],[2,4,5],[3,4,5]]}
```

which solely documents the faces, into our format, which can be seen in Table 3.

The function *calcFlow* runs a combinatorial Ricci flow on a triangulation and records the data in a file. The algorithm for solving the ODE, provided by J-P Moreau, employs a Runge-Kutta method of order 4 [7]. First, the file name for the data is provided. Then, a  $dt$  is given by the user that represents the time step for the system. The next parameter is a pointer to an array of initial weights to use. This is followed by the number of steps

Step 1	Weight	Curv	Step 50	Weight	Curv
Vertex 1:	6.000	0.7442	Vertex 1:	4.557	0.008509
Vertex 2:	3.000	-1.122	Vertex 2:	4.530	-0.01185
Vertex 3:	3.000	-1.373	Vertex 3:	4.534	-0.009091
Vertex 4:	8.000	1.813	Vertex 4:	4.563	0.01268
Vertex 5:	6.000	1.227	Vertex 5:	4.550	0.002772
Vertex 6:	2.000	-3.046	Vertex 6:	4.527	-0.01455
Vertex 7:	4.000	-0.3045	Vertex 7:	4.541	-0.003563
Vertex 8:	8.000	1.989	Vertex 8:	4.559	0.01018
Vertex 9:	5.000	0.07239	Vertex 9:	4.553	0.004906

Table 4: Two steps of a Ricci flow

to calculate and record. Lastly, a boolean is provided, where *true* indicates that the normalized differential equation, (10), should be used. Otherwise, the standard equation (4) is employed. Each step, with every vertex's weight and curvature at that step, is printed to the file. An example is shown in Table 4.

After the initial design of *calcFlow*, tests were run to determine its speed. The time it took to run was directly proportional to the number of steps in the flow. However, it was also proportional to more than the square of the number of vertices of the triangulation. As a result, while a four-vertex triangulation can run a 1000 step flow in three seconds, it would take a twelve-vertex triangulation 43 seconds to run the same flow. After inspecting the speed of the non-adjusted flow in comparison, it became clear that the calculation of total curvature, which should remain constant in two-dimensional Euclidean manifold cases, was being calculated far too often. After being adjusted so that it is calculated just once per step, the speed of the flow is much faster so that a four-vertex system with 1000 steps takes just one second and twelve vertices is much improved with a time of only four seconds. The code for the *calcFlow* function can be found in §8.5.

## 4.4 Initial testing and results

We have some expectations for combinatorial Ricci flow over two-dimensional Euclidean surfaces. Cases like the boundary of the tetrahedron can be cal-

culated by hand so it will be useful to test our results against these surfaces. For example, we expect that the tetrahedron under (4) will have all weights converge to zero. Whereas under (10) the weights are expected to converge to positive constants.

There are other expected behaviors. We expect that the *product area* will be constant at any intermediate step of the flow. Also, it is predicted that the total curvature of a 2-manifold surface should remain a constant determined by its genus.

For the program we expect to create a system that allows for easy access of information while also providing that information in a time efficient way. Our goal is to create a program that can be built upon later to provide further functionality and options without requiring widespread and time consuming changes to the code. While we certainly expect a number of bugs, we plan to develop methods to test and find any errors in our code.

Initial checks for accuracy:

1. Boundary of tetrahedron will converge to equal weights.
2. Constant *product area*.
3. Constant total curvature.

#### 4.4.1 First tests

The program for the Ricci flow was tested by beginning with the simplest cases, and then explored with as many different possibilities as we could conceive of to try to find anomalies. The first test was the boundary of the tetrahedron. In the standard equation, it is easily shown that all weights approach zero exponentially fast. In the normalized equation, and the equation that is used in the rest of the testing, the tetrahedron's weights approach a single positive number, the fourth root of the *product area* of the tetrahedron, so that the area remains constant. In addition, all the curvatures converged to the same value, in this case  $\pi$ , so that the total curvature is  $4\pi$ . Results were similar for the other platonic solids.



The next test was the torus with the standard nine-vertex triangulation. Again all the weights approached the same positive number to maintain constant area. As expected, the curvatures all went to zero while the total curvature remained zero throughout. Further simple tests included triangulations of larger genus, and in all cases the total curvature remained at a constant multiple of  $\pi$  that was expected and the *product area* was also constant. In addition, there does not appear to be any further effect from the initial weights other than determining the area of the triangulation. It is not clear from any of the tests we ran that having extremes amongst the initial weights causes a different end result.

In each case all vertices converged to the same curvature. This was not always the situation for the weights, as in many triangulations there would be several final weights. It became clear that this would occur when vertices had different degrees. In fact, we guess that there is a formula relating the *product area* of a weighted triangulation and the degree of a vertex to that vertex's final weight. In most of the examples we tried, when two vertices had the same degree, they had the same final weight, but this is not always the case. One such example is adding three vertices to one face of the tetrahedron. As seen in Table 5, vertices 4, 5, and 6 all have degree four. Yet vertex 5 has a greater final weight than the other two. The only explanation we could find with some merit is that the local vertices of 5 are different in degree from those of 4 and 6. That is, the degrees of the local vertices of 5 are never less than four, while vertices 4 and 6 each have a local vertex with degree 3. See Figure 20 in the Appendix for an illustration of weights over time.

#### 4.4.2 Morphs and specific cases

Another part of the code is a file strictly made up of functions used to manipulate and alter the triangulations being run. These functions, known within the code as *morphs*, allow us to change the triangulation in different ways, geometric as well as topological, in order to provide us with different kinds of discrete manifolds over which to run our flow.

One such example of our morphs is the use of flips, as mentioned in §2.1. We can perform 1-3, 2-2, and 3-1 flips on given triangulations and observe how those alterations affect the end flow. Flips have the special property

Vertex: 1	Vertex: 5
2 3 4 5 6 7	1 2 4 6
1 2 3 7 10 13	7 8 9 12
1 2 3 5 7 9	5 6 7 8
Vertex: 2	Vertex: 6
1 3 4 5 6 7	1 2 5 7
1 4 5 8 11 14	10 11 12 15
1 2 4 6 8 10	7 8 9 10
Vertex: 3	Vertex: 7
1 2 4	1 2 6
2 5 6	13 14 15
2 3 4	1 9 10
Vertex: 4	Edge: 1
1 2 3 5	:
3 4 6 9	:
3 4 5 6	

Final weights for a random initial weighted Triangulation
Vertex 1: 15.692
Vertex 2: 15.692
Vertex 3: 6.18421
Vertex 4: 9.6524
Vertex 5: 10.6409
Vertex 6: 9.6524
Vertex 7: 6.18421

Table 5: Adding three vertices to a Tetrahedron

that they do not change the Euler characteristic of the surface they are performed upon. For example, in performing a 1-3 flip, we have a total of 3 new edges, 2 more faces, and 1 new vertex. The value of  $\chi$  does not change as  $(V + 1) - (E + 3) + (F + 2) = V - E + F = \chi$ . This means we could do any number of these flips without changing the topology of the surface.

In addition, there are other “morphs” that can be performed to change the topology of a triangulation in order to give us some more diverse and interesting shapes over which to run these flows and observe their results. There are two such moves that we can perform.

- Adding Handles

By adding a handle to a surface, we are in essence adding a hole to it. One simple way to obtain this result is to “patch” the surface of a torus to the surface that we are working with. This is exactly what we have done. The method removes a face from the existing triangulation and replaces it with a 9-vertex triangulation of a torus. By using the three existing vertices and edges, we are actually adding 6 new vertices, 24 new edges, and 17 new faces. This operation changes the topology of

the triangulation that we are working with. It will reduce the Euler characteristic,  $\chi$ , by 2 and thus change the total curvature of the figure.

- Adding Cross-Caps

A cross-cap is a piece of a surface with a self intersection. The purpose of adding a cross-cap to a manifold is to give us a property of non-orientability. A surface of this kind is characterized by the ability to move an object along it in such a way that it reaches its original location but in mirror-image form. In this way, the portion of the surface known as the cross-cap is, itself, topologically equivalent to the mobius band. It is sufficient to add only a single cross-cap to any given surface,. In conjunction with the method of adding handles, this technique allows us to create any topology in two dimensions.

Another shape we have been looking into is called the *double triangle*. A double triangle is made of two triangles with the same three vertices. It can also be thought of as folding one triangle on top of another. We can add these to a triangulation and see how things vary with their presence. This is of interest because of their very peculiar effect on the definition of a triangulation. Without double triangles, there are certain restrictions on definitions and adjacency properties of simplices within a triangulation as outlined in the previous section on triangulations. However, with these double triangles, the restrictions are broken up by allowing double and even triple adjacency references, creating vertices with only one or two local vertices, faces with only two defining edges, and edges with only one defining vertex, among other bizarre properties. Because of these inconsistencies in definition, different surfaces that have these double triangles attached to them will behave in noteworthy ways. The function that adds these shapes takes an edge as an argument and adds another edge with the same two vertices. Then, a vertex is added and two edges are drawn from this vertex to the other two vertices mentioned. Two new faces are formed by these two new edges as well as the other two edges mentioned, one for each face. The process can be imagined as flattening a party hat and attaching it to an object along the open end.

We investigate our programs for sanctity by performing morphs on given manifolds and observe any changes in behavior. We include some examples.

*Example:* Adding a vertex to a one-holed torus. See figure 11.

By inserting a vertex within a triangulation for a torus, we are essentially creating a bump on the torus and then observe what happens as we run it through out *calcFlow* program. We discovered that the new vertex shrinks in size to a weight much smaller than the other vertices, but to a positive constant. To counter this, the other vertices grow slightly to maintain Eq. (7). The weight that the new vertex converges to turned out to be in proportion to the other weights by  $3 + 2\sqrt{3}$ , the exact proportion necessary to maintain equality amongst all other weights. An oddity here is that the three vertices local to this added vertex converged to the same weight as all the vertices not near the flip, despite a difference in degree.

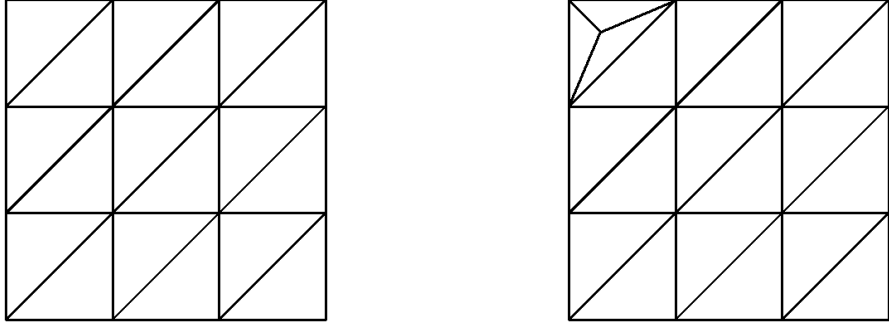


Figure 11: A triangulation of the torus, and the addition of a new vertex. This is a 1-3 flip.

*Example:* Adding a leaf to a two-holed torus.

When we added a double triangle to the edge of a two-holed torus, we experienced for the first time what is known as a singularity. At the special vertex that was only of degree two, its weight continued to shrink and never converged. Eventually, enough steps of the Ricci flow were performed that the size of the weight became less than what the computer could differentiate from 0 and the program crashed with a division-by-zero error. Before the crash, the other vertices were increasing without convergence to counteract the decreasing weight. The reason is that all vertices wanted to attain the same curvature, in this case  $-\frac{2}{5}\pi$ . Yet the new vertex, with only two angles

in its sum, can only obtain a curvature of 0 (each angle  $\sim \pi$  radians). The result is that the weight shrinks in an attempt to attain angles greater than  $\pi$ , which is simply not possible. What is still not clear is whether or not the weight reaches 0 in finite time, or simply approaches 0. This is difficult to test with a computer only capable of approximating the weight, though we expect that it does so in finite time.

*Example:* Performing a 2-2 flip on a 12-vertex torus.

One interesting observation we made was that flips can drastically change the behavior of some triangulations. For Example, in a 12-vertex torus, performing a flip on one edge affected created a double triangle. Similarly to the previous case, all curvatures are converging to 0, but the vertex with degree 2 simply cannot accomplish this. However, unlike the previous case, we suspect that the weight does not become 0 in finite time, but instead approaches 0.

*Example:* Triangulation of genus 4.

While the previous two cases were quite interesting, there is some hesitation given that we were using double triangles and being less restrictive in what were allowable triangulations. But the theory behind why both situations reacted as they did left hope for a case that fit in a stricter setting. In the same sense that a two degree vertex could have a curvature no less than 0, a three degree vertex is bounded below by  $-\pi$ . It was observed that the vertices of a triangulation all converge to  $\frac{2\pi\chi}{|V|}$  curvature. Now it was a matter of finding a triangulation with a large enough genus and few vertices. The first we found, provided by [5], was an 11 vertex triangulation with genus 4. To create a vertex with degree 3, we chose to add a new vertex to a face with a 1-3 flip. This made all curvatures try to converge to  $-\pi$ . We then expected that the new vertex would react as in the previous example. This was in fact the case, and it presents the question of whether or not there is a limit on the degree that can create such a singularity. The issue being that for higher genus, more vertices are required. Unfortunately, [5] does not provide large enough triangulations for fourth degree vertices. A data plot of this similar situation with a genus 6 triangulation is provided in §8.4.

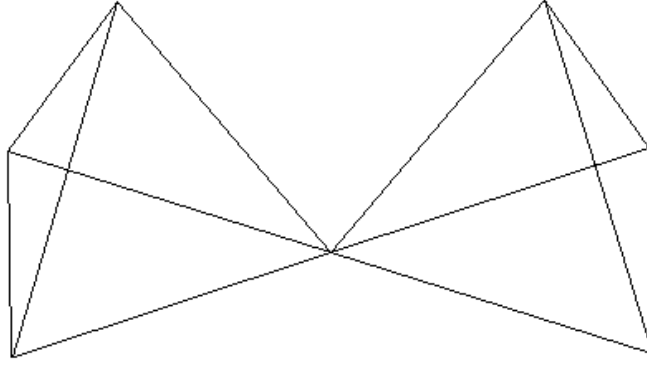


Figure 12: Two tetrahedra conjoined at a vertex.

*Example:* Two tetrahedra connected at a vertex. See Figure 12

It turns out  $\chi = 7 \text{ Vertices} - 12 \text{ Edges} + 8 \text{ Faces} = 3$ , which is not a case we had seen before. Technically, this example contradicts our notion of a manifold, but we felt it useful in validating our program procedure. Starting each vertex with equal weight, we obtained a somewhat unexpected result. The center weight becomes very large, and the others become smaller in comparison. We concluded that since the central vertex has a much higher degree, its weight becomes large, creating elongated tetrahedra on either side, in order to have the same curvature as all other vertices. One good thing we noted was that the total curvature equaled  $6\pi = 2\pi\chi$ .

#### 4.4.3 Convergence speeds

One experiment we performed was measuring convergence speeds of various triangulations. For each triangulation, five flows were run where the weights were random between one and twenty-five. Random weights, while not a perfect solution, was the most effective option and easiest to implement. It was unclear what set weights could have an equal effect for different triangulations. By performing five trials and using random weights, we hope to negate

any effect the weights could have on the convergence speed of a triangulation. The  $dt$  was held constant at 0.03 so that the number of steps needed to run was not large and time consuming and still provided accurate results. For each run, a step number was assigned for when all weights and curvatures had converged to four digits, (the precision shown in a file of the results).

Beginning with the basic case, the tetrahedron took on average 156.8 steps to converge to four digits and remained fairly consistent through all five trials. Strangely, the octahedron converged faster on all five flows, averaging 138.4 steps. This was made all the stranger by the fact that the icosahedron averaged 198.8 steps. The torus revealed several things about convergences. First, the standard nine vertex torus averaged only 110 steps, suggesting that a torus converges faster than a sphere. When a vertex was added to the torus, it greatly decreased the convergence speed, to 248.8 steps. Compared to the Tetrahedron with an added vertex, 164.2, this was a very large jump. When another vertex was added to the same face as the first, the convergence speed dropped yet again, to an average of 437.6 steps. Yet when this vertex was added to a face not connected to the first, the convergence speed was almost steady at 264.8. And adding a third in the same style caused little increase.

This seems to suggest that convergence speed is dependent on the number of unique vertices. By unique we mean the properties of the vertex (number of local vertices, the weight it converges to, etc.). When the vertices were added to separate faces, there remained only three unique vertices. Whereas, adding the two vertices to the same face created five unique vertices. This theory is further supported by a twelve vertex sphere designed so that all vertices are unique. The average convergence was 460 steps, more than twice as long as the icosahedron, which also is a twelve vertex sphere.

As a final note, the deviation of the initial weights did not have a clear impact on the convergence speed. At some times, it would appear that initial weights with a higher deviation would converge faster, yet at other times it was lower deviation that seemed to lead to faster convergence.

Using dt = 0.03			Random between 1 - 25		
Triangulation	Trial	Steps to converge to four digits	Triangulation	Trial	Steps to converge to four digits
Tetrahedron	1	159	Octahedron	1	127
	2	166		2	153
	3	157		3	134
	4	151		4	136
	5	151		5	142
	Average:	156.8		Average:	138.4
Icosahedron	1	217	Torus-9	1	112
	2	179		2	112
	3	209		3	109
	4	172		4	108
	5	217		5	109
	Average:	198.8		Average:	110
Tetrahedron with added vertex	1	181	Octahedron with added vertex	1	230
	2	156		2	232
	3	156		3	234
	4	131		4	193
	5	197		5	243
	Average:	164.2		Average:	226.4
Torus-9 with added vertex	1	265	Tetrahedron with two added vertices on face 1	1	202
	2	181		2	232
	3	254		3	224
	4	275		4	227
	5	269		5	190
	Average:	248.8		Average:	215
Torus-9 with two added vertices on face 1	1	433	Torus-9 with two added vertices on face 1 and 5	1	264
	2	421		2	245
	3	468		3	244
	4	442		4	269
	5	424		5	302
	Average:	437.6		Average:	264.8
Torus-9 with three added vertices on face 1 and 5 and 9	1	272	Tetrahedron with two added vertices on face 1 and 2	1	189
	2	270		2	183
	3	297		3	174
	4	291		4	190
	5	231		5	232
	Average:	272.2		Average:	193.6
Tetrahedron with flip	1	209	Octahedron with flip	1	200
	2	299		2	210
	3	204		3	225
	4	281		4	182
	5	262		5	237
	Average:	251		Average:	210.8
Torus-9 with flip on edge 1	1	107	12-vertex sphere with all different convergences	1	565
	2	131		2	373
	3	134		3	486
	4	116		4	503
	5	138		5	373
	Average:	125.2		Average:	460

Figure 13: Summary of convergence data for varying criteria



## 5 Spherical and hyperbolic Ricci flow

So far we have focused exclusively on triangulations using Euclidean geometry. While this is useful for most cases, there are others where a different background space may be better suited. Two of these in particular are spherical and hyperbolic geometries. We will introduce the basics of each system to the reader as they may be unfamiliar with these geometries. We will examine the adaptations of combinatorial Ricci flow for each case, test over various triangulations, and attempt to reach conclusions on our findings.

### 5.1 Spherical flow

If you were to draw a large triangle on the surface of the earth, you would see that the line segments are no longer linear, but follow along an arc. In dealing with spherical geometry, we learn that many rules of planar geometry, some of them fundamental, do not apply. To begin, the sums of angles in a triangle do not add to  $180^\circ$ . The sum changes depending on the edge lengths. For computational reasons, we cannot (easily) have edges of unbounded length. While we can assume our circle packing metric still holds, we do have additional restrictions:

- All triangles must be producible on a sphere of radius 1, the unit sphere.
- By default, we imply the geodesic of a spherical triangle, using the shortest distance on the surface between any two vertices. As a result, the sum of the weights of any triangle cannot exceed  $\pi$ . In addition to contradicting the previous definition, such a situation can lead to undefined calculations of our angles, the equation of which is provided below.

We also have different formulas for numerous things in the spherical case. There are now two laws of cosines. One gives you an angle based on the edge lengths, like in Euclidean space, and the other gives you the side lengths based on the angles. For the first law of cosines, given a triangle with edge lengths  $a, b$ , and  $c$ , we have  $\cos(\angle C) = \frac{\cos(c) - \cos(a)\cos(b)}{\sin(a)\sin(b)}$ . Using Taylor polynomials to a couple of terms, we can see that this is analogous to the Euclidean version.

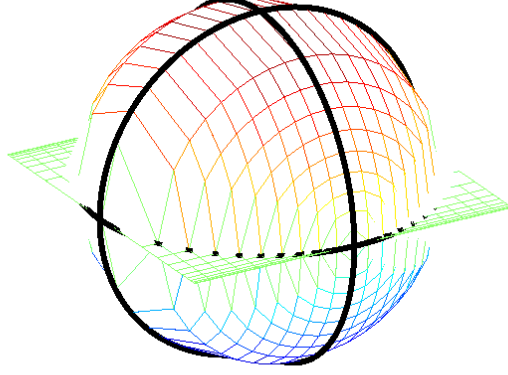


Figure 14: An illustration of a spherical octahedron through the X-Y plane. Each octet of the sphere surface, outlined in black, is the face of one triangle.

With  $\sin(x) \approx x$  and  $\cos(x) \approx 1 - \frac{x^2}{2}$  for  $x$  small, we get

$$\begin{aligned}
 \cos(\angle C) &= \frac{\cos(c) - \cos(a)\cos(b)}{\sin(a)\sin(b)} = \frac{(1 - \frac{c^2}{2}) - (1 - \frac{a^2}{2})(1 - \frac{b^2}{2})}{ab} \\
 &= \frac{\frac{a^2}{2} + \frac{b^2}{2} - \frac{c^2}{2} + \frac{a^2b^2}{4}}{ab} \\
 &= \frac{a^2 + b^2 - c^2}{2ab} + \frac{ab}{4} \approx \frac{a^2 + b^2 - c^2}{2ab} \text{ as } \frac{ab}{4} \approx 0 \text{ for } a, b \text{ small}
 \end{aligned}$$

More importantly, our equation for combinatorial Ricci flow is altered slightly. The base equation, as given by [2], is now

$$\frac{dr_i}{dt} = -K_i \sin(r_i). \tag{11}$$

Like in the Euclidean case, we see the possibility that all weights could continually decrease towards zero. However, scaling in the spherical case is not quite as easy as before: the angles are affected by the change in edge lengths. Plus, we also need to make sure that the weights remain within bounds.

We tried a few techniques to derive an equation for normalized spherical flow. Some ideas were:

- $\frac{dr_i}{dt} = (\bar{K} - K_i) \sin(r_i)$

By maintaining the same construction as the normalized Euclidean Ricci flow, we hoped that replacing  $r_i$  with  $\sin(r_i)$  would work. However, in running even the simplest case of a tetrahedron, we found that the system was highly unstable. If more than one weight was initially different from the others, the program would fail. If the system was able to stabilize, we noted that the resultant surface area of the end product was  $4\pi$ , the same as a unit sphere. Another issue with this formula is that the value  $\bar{K}$  is no longer constant. For a spherical construction of a surface  $X$ , we have

$$\bar{K} = \frac{\sum K_i}{|V|} = \frac{2\pi\chi - \text{Surface Area of } X}{|V|}.$$

This is known as the Gauss-Bonnet theorem and is noted in Chow and Luo's paper [2]. Since the surface area went to  $4\pi$ , then the average curvature went to zero. While we liked the end result of our triangulation trials, the system failed far too often to be reliable.

- $\frac{dr_i}{dt} = (\hat{K} - K_i)r_i$

Following the criteria we used to obtain our normalized Euclidean flow, we began experimenting and used the cases  $\tilde{r}_i = \alpha r_i$  and  $\prod \alpha \sin r_i = C$  to obtain a result similar to our original. We defined  $\hat{K}$  as the dot product of the curvatures and the cosines of the weights, divided by the number of vertices, or

$$\hat{K} = \frac{\sum K_i \cos r_i}{|V|}.$$

The major problem we encountered with this formula was that we had to use a sine approximation in its derivation, which is not valid for larger weights. As angles are not conserved with scaling in the spherical case, we realized this formula would not work. We also found that weights and curvatures displayed sinusoidal behavior, but were unable to converge to a finite value. As time went on, the weights became more unstable until the program reached failure, as seen in Fig. 15.

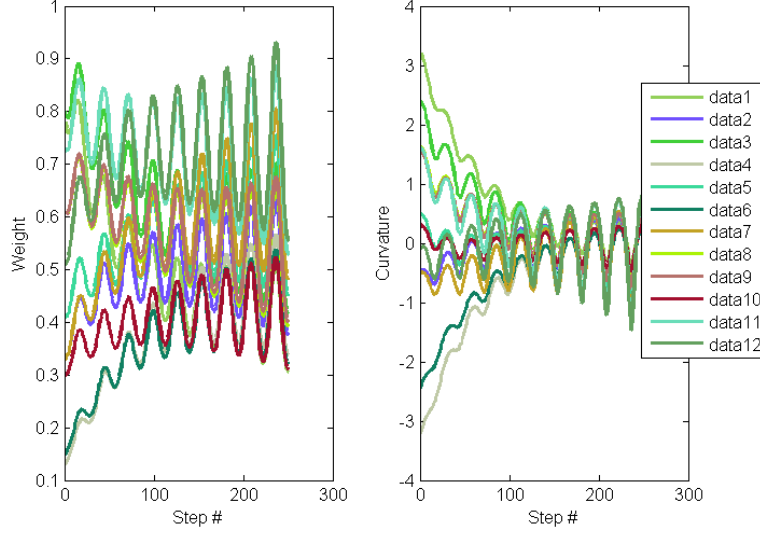


Figure 15: An example using our notion of  $\hat{K}$ . Weights and curvatures were unable to converge, and crashed the program shortly after.

In the end, we decided to try an equation that took the good aspects of our first trial while broadening its range of stability as we had hoped with the second one. We came up with the equation

$$\frac{dr_i}{dt} = \bar{K}r_i - K_i \sin(r_i). \quad (12)$$

The basing for this equation was applying (6) to the standard Spherical equation and recognizing that the average curvature component should likely not be the sine of the weight, but just the product of the weight itself. Unfortunately, we have no proof that this equation is truly valid or that its design is backed in rigorous mathematics. However, in examining its behavior with various triangulations, we found that this one works very well. By this we mean that the results were consistently in a form that was expected or appeared to be reasonable, or otherwise acted similarly to that of the Euclidean normalized flow. We find that spheres converge to zero curvature and weights first group together and then approach optimal weights. See Figure 16.

In dealing with vertex transitive triangulations, ones in which each vertex has the same degree, we noted that sometimes all weights would converge to a specific value that was dependant on the number of vertices, and sometimes all the weights would be close to this number but off by a small amount. In either case, the resulting surface area at the end turned out to be  $4\pi$ . For a vertex transitive genus 0 surface, we found that the preferred weight that each vertex approached or reached was equal to

$$r_i = \frac{1}{2} \arccos\left(\frac{\cos(Z)}{1 - \cos(Z)}\right) \text{ where } Z = \frac{\pi(4 + F)}{3F}$$

and  $F$  is the number of faces of the given triangulation. For example, with a tetrahedron,  $F = 4$ ,  $Z = \frac{2\pi}{3}$ , and  $r_i = \frac{1}{2} \arccos(-\frac{1}{3}) \approx 0.9553$ . The only downsides we found with this equation were that it was still possible for the system to fail if some weights got too large, and the computation time required to reach a stable equilibrium was lengthier than expected. Looking at Fig. 16, we see that with the  $dt$  size given of 0.5, it would take over 500 steps for the system to reach equilibrium, and this would be much longer with the  $dt$  used in §4.4.1.

## 5.2 Hyperbolic flow

In hyperbolic geometry, we encounter a new background that has properties both similar and distinct from Euclidean and spherical systems. A common way to visualize the hyperbolic plane can be seen in Fig. 17. This representation is often called the Poincaré disk, named after the same Poincaré as in §4.

There are several interesting properties with the hyperbolic plane. We now have that for a line  $l$  and a point  $P$  not on that line, there are an infinite number of lines through  $P$  that do not intersect  $l$ . In Euclidean geometry, such a line is unique. The shortest distance between two points is still a straight line, but illustratively can be found by following a curved path along a circle centered at infinity going through both points. A more thorough explanation of hyperbolic geometry can be found in most college geometry textbooks.

In terms of the formulas, they remain relatively similar in format to the spherical equations, except there are two main substitutions. The cosine and sine functions are often replaced with their hyperbolic counterparts  $\cosh$  and

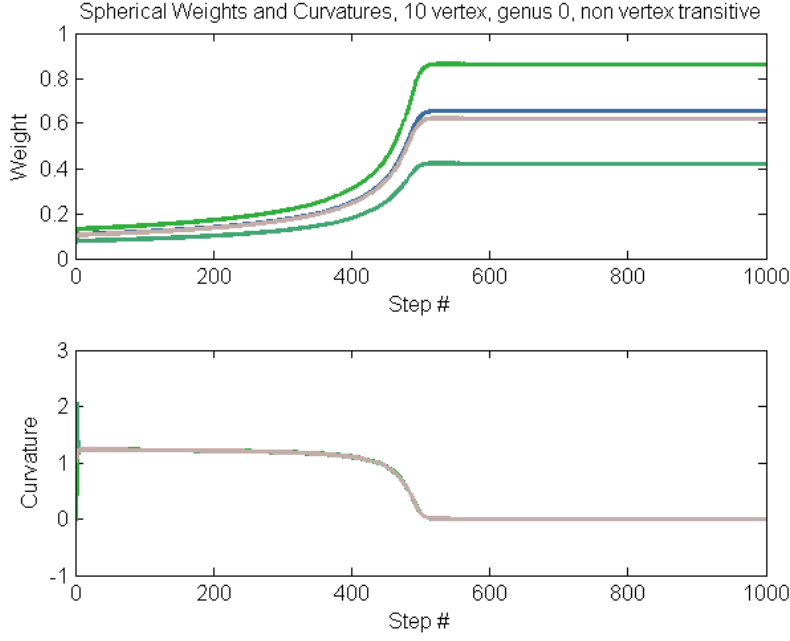


Figure 16: An example of a solution using Eq. (12). Starting off with equal initial weights of 0.1, vertices merge into one of four groups as they approach uniform curvature relatively quickly. As curvature drops to zero, slowly at first but more forcefully as time passes, the weight groups separate from each other to obtain their final weight. In this trial,  $dt = 0.50$  to show the complete process.

$\sinh$ , defined as

$$\begin{aligned}\sinh(x) &= \frac{e^x - e^{-x}}{2} \\ \cosh(x) &= \frac{d \sinh(x)}{dt} = \frac{e^x + e^{-x}}{2}\end{aligned}$$

Most importantly, the equation for combinatorial Ricci flow is now

$$\frac{dr_i}{dt} = -K_i \sinh(r_i) \quad (13)$$

Like in the case of spherical flow, the average and total curvatures need not

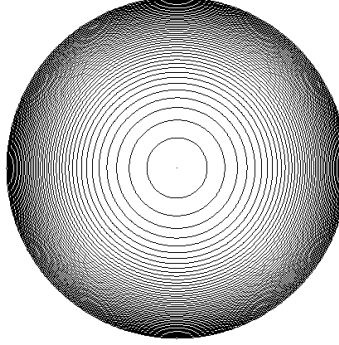


Figure 17: An illustration of the hyperbolic plane using the Poincaré disk. All concentric circles are evenly spaced apart in a Euclidean background, but the outer edge of the disk approaches infinity, so the circles appear closer together. A similar way to think of it is to imagine looking at the contour graph of  $z = x^2 + y^2$  from the point  $(0,0,-1)$ .

remain constant. The average curvature is now

$$\overline{K} = \frac{\sum K_i}{|V|} = \frac{2\pi\chi + \text{Surface Area of } X}{|V|}.$$

After running the hyperbolic Ricci flow on a few samples, we noted that the weights did not always go to zero, as was the case with the previous unnormalized systems. So in some cases, it almost seems as if this equation is already normalized. Curvatures would converge to zero, and optimum, nonzero weights are achieved in a relatively short time. Other times it behaved like both Euclidean and spherical.

### 5.3 Comparison of Systems

When we began looking into these background geometries, we thought that it would be a good idea to run uniform tests on all three systems. We could observe whether or not each triangulation converges in the same fashion, or if it matters which geometry we choose. If we do discover that all systems behave the same way, we would then like to focus on one geometry, most likely Euclidean. However, since our equation for normalized spherical Ricci

flow is not wholly confirmed as the best method, and as the hyperbolic flow may or may not already be normalized, we can not make any strong conclusions on the normalized flows. We did decide, however, to take a look at the behaviors on various manifolds by using the non-normalized equations, (4), (11), and (13). We will look at three triangulations, each of a different genus, without performing any morphs, and compare results between each system.

In terms of programming these new flows, we were able to adapt our *calcFlow* program into two new programs, *sphericalCalcFlow* and *hyperbolicCalcFlow*, to easily distinguish which background we were using. This way we could run the systems one at a time, or all at once and observe differences in their behaviors in cases with the same initial conditions.

*Example:* 12 vertex sphere, vertex transitive of degree 5

Euclidean- As expected, we obtain a surface where all the vertices attain the same curvature of  $\frac{\pi}{3}$  after multiple trials of uniform and randomized weights. The weights group together somewhat as in the normalized spherical case, and then continue decreasing towards zero.

Spherical- We found that the system was truly stable with nonzero final weights if and only if all initial weights were set exactly to its preferred weight, which is  $\approx 0.55357$  based on the fact that this triangulation has 20 faces. If the initial curvature was below zero, the weights would increase rapidly until the program crashed. If the initial curvature was positive, the vertices would approach the same curvature as in the Euclidean case. In doing so, the weights would drop to zero.

Hyperbolic- We found that the vertices react in a similar manner to the Euclidean case. They approach the same curvature of  $\frac{\pi}{3}$  and drop towards zero weights at the same rate.

*Example:* 9 vertex, one-holed torus

Euclidean- Since we know that  $\chi = 0$  for a one-holed torus, we also know that  $\overline{K} = 0$  and so each vertex obtains zero curvature. The weights do not drop to zero, but converge to positive values reflective of their degree.



Spherical- We found this system to be very unstable with the torus. If the initial weights were too large, we found that the total curvature would be well below zero, and the weights would continually increase until spherical-`CalcFlow` crashed. While we hoped that reducing the initial weights would bring stability to the system, we ended up with the same result.

Hyperbolic- While the total curvature of the system goes to zero, the weights also approach zero but maintain roughly the same proportion as the final Euclidean weights. Another thing we noted was the time required for the weights and curvatures to go to zero. This system was extremely slow and took much longer than either the Euclidean or spherical trials.

*Example:* 11 vertex, two-holed torus

Euclidean- As in previous cases, the vertices converge to a uniform curvature. However, as this value was negative (given  $\chi = -2$ ) we saw the weights increase without bound. As there is no limit to the weights in the Euclidean case, `calcFlow` had no troubles calculating each iteration, but having unbounded weights is still an undesired result.

Spherical- Regardless of the initial weights, we found that the total curvature of the system would continually decrease, and as such the weights of each vertex would increase until `sphericalCalcFlow` crashed.

Hyperbolic- Here we found that hyperbolic geometry was very effective. In a very short time, we saw the vertices reach zero curvature, and the weights converge to nonzero values. This is how we got our notion that the hyperbolic Ricci flow was already normalized. This also coincides with the suggestion in [2]; when working with a negative euler characteristic manifold, one should use hyperbolic geometry.

To conclude, we generalize that certain flows work best for triangulations whose total curvature goes to zero in that particular system. Euclidean is best for systems of genus 1, or one-holed tori. Spherical combinatorial Ricci flow is said to work best on manifolds of genus 0, or anything topologically equivalent to a sphere. This is because we have a positive  $\chi$  value, so for total curvature to go to 0, the total surface area must go to  $4\pi$ . Spherical was the only system that could have produced a nontrivial solution in our first example. Hyperbolic Ricci flow is best suited for triangulations with a

genus of 2 or more. We can see that these systems will be able to reach zero total curvature with a large enough surface area.

## 6 Future work

### 6.1 Linking Delaunay to Ricci flow

Delaunay surfaces and combinatorial Ricci flows can seem to be very separate concepts, and in many ways with our program structure, they are. Yet there is the possibility of combining both of them to explore other mathematical inquiries. For instance, how does the idea of Delaunay triangles interact with triangulations on a manifold. We know that a circle packed triangulation is weighted Delaunay, but what if the triangulation is not circle packed (see below)? Will the Ricci flow lead to a weighted Delaunay triangulation?

### 6.2 Circle packing expansions

Circle packing is a very special way to characterize our side lengths. If we relax this criteria and let the circles overlap, we can introduce a second weight  $\Phi$  that is representative of the angle of their intersection. See Figure 18. We can then evaluate our side lengths as

$$l_{ij} = \sqrt{r_i^2 + r_j^2 + 2r_i r_j \cos(\Phi(e_{ij}))}$$

With this more general interpretation, we can exa questions asked by Chow and Luo in [2].

### 6.3 3-Dimensional triangulations

Triangulations exist outside of two dimensions and one future goal is to perform flows in a three dimensional setting. The flow in this case is known as Yamabe flow, discussed in [3]. While Yamabe flow is similar to Ricci flow, its value of  $K_i$  is determined quite differently, involving not only the angles of the faces, but also the cone angles associated with tetrahedron vertices. The structure is in place from this project to accomplish this goal. To help the understanding of both the two and three dimensional triangulations, we would like to create a way to visualize them and explore the surfaces locally.

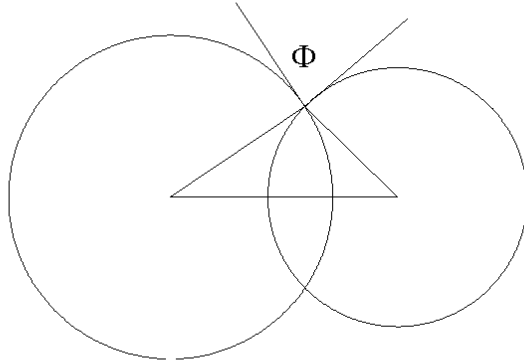


Figure 18: An example of relaxing circle packing and introducing  $\Phi$ .

## 7 Conclusion

There were many things we wanted to explore with triangulations, particularly towards Delaunay surfaces and combinatorial Ricci flow. A major aspect of our research was the creation of a functional and adaptable program to provide meaningful data. We feel that we have accomplished this goal. We have added a user interface to the program (see §8.5) for a straightforward way to run flips or flows. We hope that in the future this program can be used by others to perform their own tests.

Our work on Delaunay surfaces is unfinished, but we are excited about the prospects introduced by negative triangles. The research performed in this paper is the beginning of what we hope is a development of these negative triangles and of universally accepted definitions about them. In combinatorial Ricci flow, we have helped confirm the assertions given by [2] with numerical results in the Euclidean case. We have seen how certain properties of a weighted triangulation behave under combinatorial Ricci flow such as the weights and curvatures. Under Spherical geometry we remain uncertain as to the validity of our normalized Ricci flow, but are optimistic that such a formula does exist. Along with the above mentioned areas of further work, we also propose research in 3-dimensional Yamabe flow and in Delaunay al-

gorithms on manifolds.

In addition to the clearly defined goals in the paper, we were able to experience a large scale project that often required independent work. We also became knowledgeable in an area of mathematics that is still young in its development. For these things we would like to thank Dr. David Glickenstein for being our mentor and guide on this project, Dr. Robert Indik and the University of Arizona Math Department for their help and support, and the National Science Foundation VIGRE #0602173.

## References

- [1] M. Brown. *Ordinary Differential Equations and Their Applications*. Springer-Verlag, New York, NY, 1983.
- [2] B. Chow and F. Luo. *Combinatorial Ricci Flows on Surfaces*. Journal of Differential Geometry 63, Volume , 97-129, 2003.
- [3] D. Glickenstein. *A combinatorial Yamabe flow in three dimensions*. Topology 44, 791-808, 2005.
- [4] D. Glickenstein. Geometric triangulations and discrete laplacians on manifolds. Material given to us by David, 2008.
- [5] F. H. Lutz. The manifold page. <http://www.math.tu-berlin.de/diskregeom/stellar/>.
- [6] Dana Mackenzie. The Poincaré conjecture proved. <http://www.sciencemag.org>.
- [7] J-P Moreau. Differential equations in c++. [http://pagesperso-orange.fr/jean-pierre.moreau/c\\_eqdiff.html](http://pagesperso-orange.fr/jean-pierre.moreau/c_eqdiff.html).

## 8 Appendix

### 8.1 Derivation of Eq. (8)

We used the criteria

$$f(\tilde{r}_1, \tilde{r}_2, \dots, \tilde{r}_n) = \prod \tilde{r}_i = \prod \alpha r_i = \alpha^n \prod r_i = C$$

to constrain the values of radii. We take the derivative of  $f$  with respect to  $t$  and obtain

$$\begin{aligned} \frac{df}{dt} &= n\alpha^{n-1} \frac{d\alpha}{dt} r_1 r_2 \dots r_n + \alpha^n \frac{dr_1}{dt} r_2 r_3 \dots r_n \\ &+ \alpha^n r_1 \frac{dr_2}{dt} r_3 r_4 \dots r_n + \dots + \alpha^n r_1 r_2 \dots r_{n-1} \frac{dr_n}{dt}. \end{aligned}$$

But since  $\frac{dr_i}{dt} = -K_i r_i$  from Eq. (4) we obtain

$$\begin{aligned} \frac{df}{dt} &= \frac{n\alpha^n}{\alpha} \frac{d\alpha}{dt} r_1 r_2 \dots r_n - K_1 \alpha^n r_1 r_2 r_3 \dots r_n \\ &- K_2 \alpha^n r_1 r_2 r_3 r_4 \dots r_n - \dots - K_n \alpha^n r_1 r_2 \dots r_{n-1} r_n \end{aligned}$$

from which we can group terms and obtain

$$\begin{aligned} \frac{df}{dt} &= (\alpha^n r_1 r_2 \dots r_n) \left( \frac{n}{\alpha} \frac{d\alpha}{dt} - K_1 - K_2 - \dots - K_n \right) \\ &= C \left( \frac{n}{\alpha} \frac{d\alpha}{dt} - K_1 - K_2 - \dots - K_n \right). \end{aligned}$$

If we assume the product is a constant, we have  $\frac{df}{dt} = 0$ . Thus we have

$$\frac{n}{\alpha} \frac{d\alpha}{dt} - K_1 - K_2 - \dots - K_n = 0.$$

Rearranging we have

$$\frac{1}{\alpha} \frac{d\alpha}{dt} = \frac{d(\log \alpha)}{dt} = \frac{K_1 + K_2 + \dots + K_n}{n} = \overline{K}$$

which we refer to as Eq. (8)

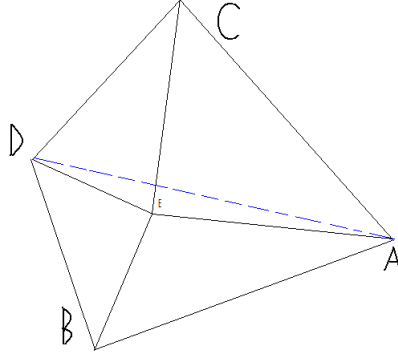


Figure 19: An illustration associated with our proof of Proposition 1.

## 8.2 Proof of Proposition 3.1

The sum of the opposite angles on a non-Delaunay hinge is greater than  $\pi$ .

*Proof.* Let  $\triangle ABC$  and  $\triangle BCD$  be triangles with common edge  $\overline{BC}$ . Let  $r$  be the radius of the circumcircle of  $\triangle ABC$  and  $E$  be the center of that circle. Then we wish to show that if  $\overline{DE}$  is less than  $r$ , then  $\angle BAC + \angle BDC > \pi$ .

We know that  $\overline{AB} = \overline{AE} = \overline{EC} = r$ , so  $\angle EBA = \angle BAE$  and  $\angle EAC = \angle ACE$ . Therefore,  $\angle EBA + \angle ACE = \angle BAC$ .

We first consider  $\overline{DE} = r$ . Then similar to above,  $\angle EBD = \angle BDE$  and  $\angle EDC = \angle DCE$ , so  $\angle EBD + \angle DCE = \angle BDC$ . Thus,  $\angle BAC + \angle EBA + \angle ACE + \angle BDC + \angle EBD + \angle DCE = 2\angle BAC + 2\angle BDC = 2\pi$  since  $ABCD$  is a quadrilateral. So  $\angle BAC + \angle BDC = \pi$ .

Now we suppose  $\overline{DE}$  is less than  $r$ . So  $\angle BDE > \angle EBD$  and  $\angle DCE > \angle EDC$ . Therefore we have

$$\begin{aligned} \angle BAC + \angle EBA + \angle ACE + \angle BDC + \angle EBD + \angle DCE &= 2\pi \\ \Rightarrow 2\angle BAC + 2\angle BDC &> 2\pi \quad \Rightarrow \angle BAC + \angle BDC > \pi. \end{aligned}$$

Hence the sum of the opposite angles on a non-Delaunay hinge is greater than  $\pi$ .  $\square$

### 8.3 Remarks on Runge-Kutta method for solving Eq. (10)

The method used by Moreau in [7] to solve a differential equation involves using a Runge-Kutta method. Prior to adapting the code from Moreau's website, we reached the conclusion that a Runge-Kutta format would be most beneficial for this type of differential equation problem. Even though it is more computationally complex than the simpler Euler's method, it makes up in its ability to converge and in its accuracy. According to [1] the error associated with using Runge-Kutta is on the order of  $h^4$ , whereas with a standard Euler approximation the error is simply of order  $h$ , with  $h = dt$  being our step incremental.

Based on our evaluations of radii and curvatures over time, it appears to converge exponentially for each vertex. However, as mentioned previously, performing flips on a triangulation may create unusual behavior.

### 8.4 Data Plots

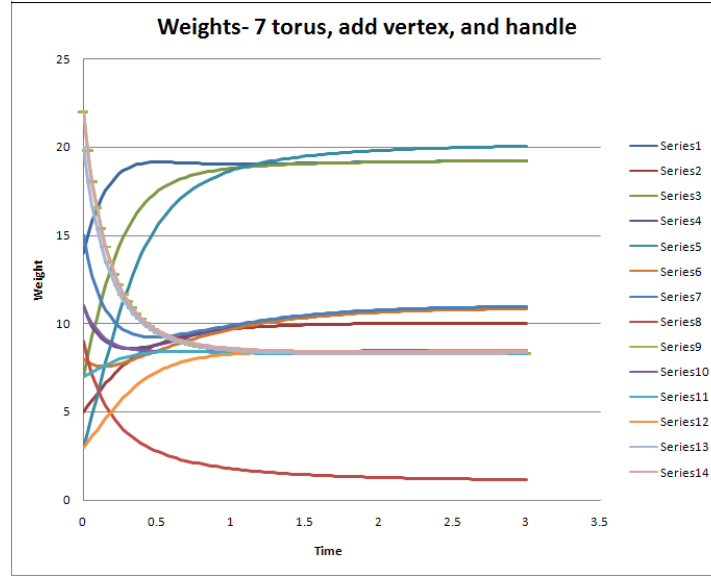


Figure 20: An example of how morphs can change the asymptotic behavior of vertices. In this case we saw the weights of some vertices change concavity.



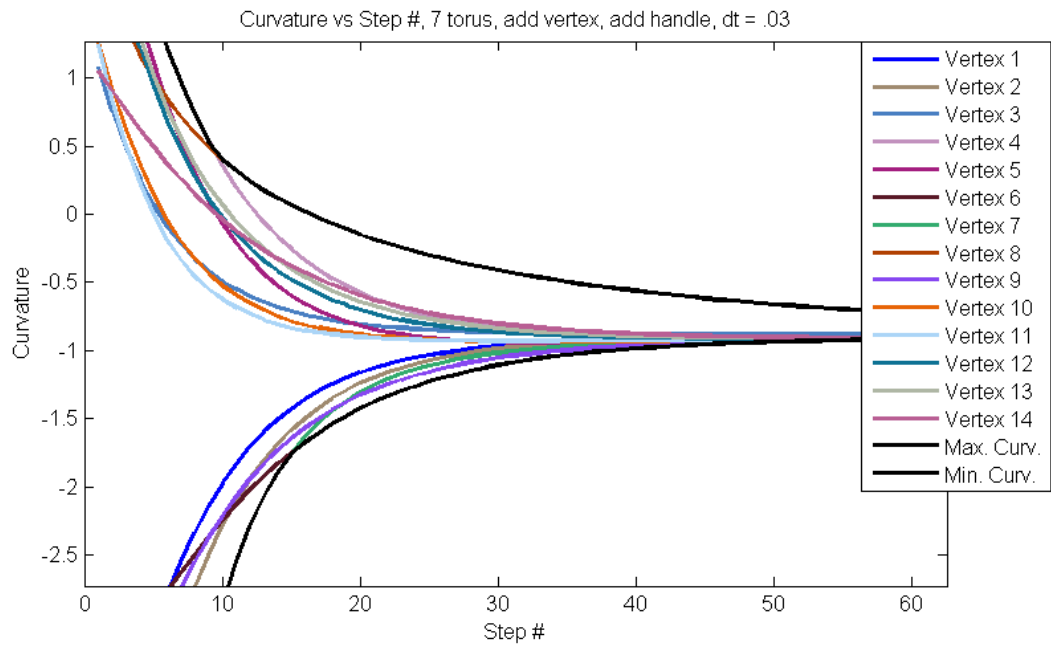


Figure 21: An example of curvatures over time. While they do converge to the same curvature, the vertex with the maximum or minimum curvature may change. This is a separate trial than that producing Fig. 20

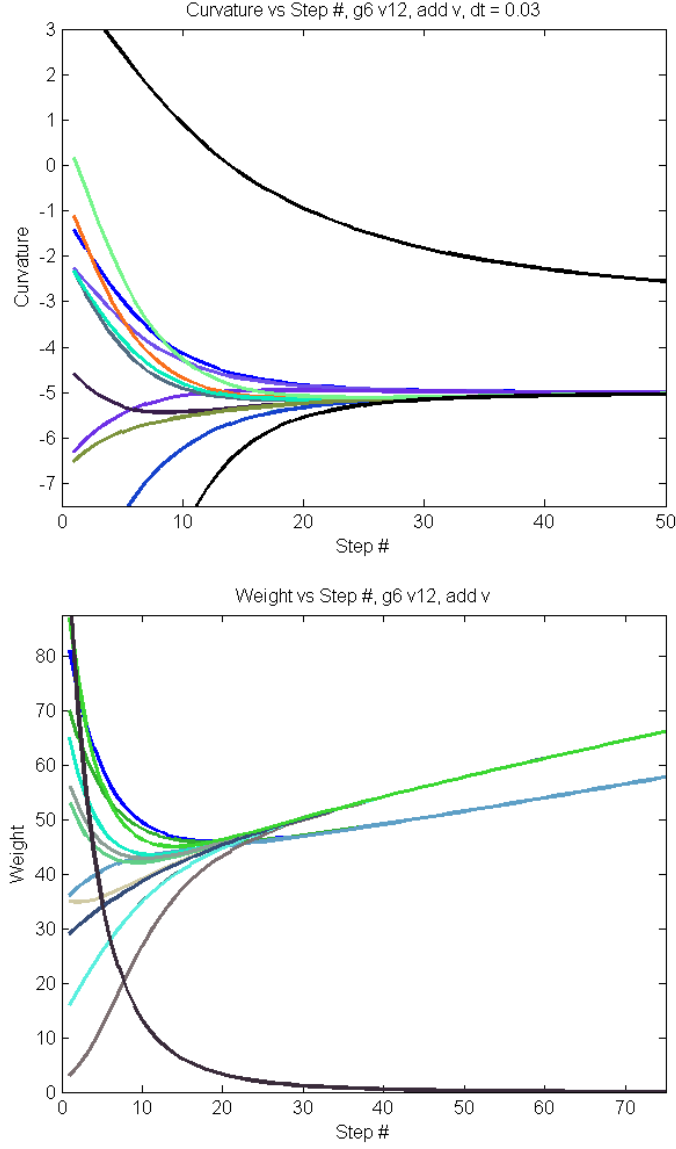


Figure 22: An example of adding a vertex to a genus 6 surface. One of the curvatures is unable to drop below  $-\pi$ , and as a result, its weight is pushed to almost zero. Other vertices group together to compensate for this behavior.

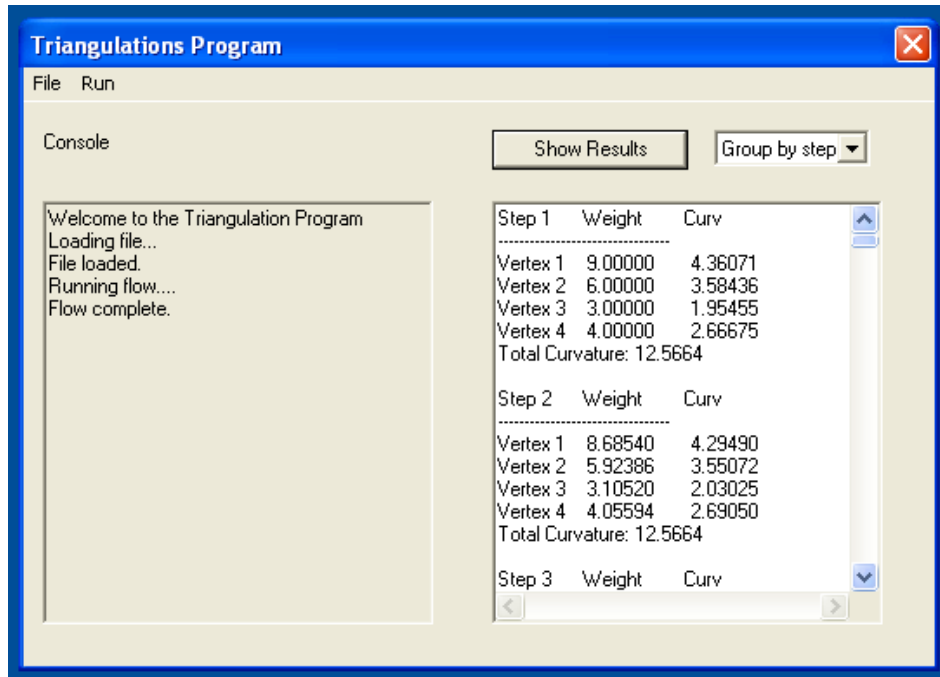


Figure 23: A snapshot of the user interface written to run both Ricci flows and Delaunay flip algorithms. Results of a flow are written in a text field on the right.

## 8.5 Code Examples

Code from the program can be found here: <http://code.google.com/p/geocam>.

The *clacFlow* method calculates the combinatorial Ricci flow of the current Triangulation using the Runge-Kutta method. Results from the steps are written into vectors of doubles provided. The parameters are:

- **vector<double>\* weights-** A vector of doubles to append the results of weights, grouped by step, with a total size of  $\text{numSteps} * \text{numVertices}$ .

- **vector<double>\* curvatures-** A vector of doubles to append the results of curvatures, grouped by step, with a total size of numSteps \* numVertices. The time step size. Initial and ending times not needed since diff. equations are independent of time.
- **double\* initWeights-** Array of initial weights of the Vertices in order.
- **int numSteps-** The number of steps to take. ( $dt = (tf - ti)/numSteps$ )
- **bool adjF-** Boolean of whether or not to use adjusted differential equation. True to use adjusted.

The information placed in the vectors are the weights and curvatures for each Vertex at each step point. The data is grouped by steps, so the first vertex of the first step is the beginning element. After n doubles are placed, for an n-vertex triangulation, the first vertex of the next step follows. If the vectors passed in are not empty, the data is added to the end of the vector and the original information is not cleared.

```
void calcFlow(vector<double>* weights, vector<double>* curvatures, double dt,
             double* initWeights, int numSteps, bool adjF)
{
    int p = Triangulation::vertexTable.size(); // The number of vertices or
                                                // number of variables in system.

    double ta[p],tb[p],tc[p],td[p],z[p]; // Temporary arrays to hold data for
                                         // the intermediate steps in.
    int    i,k; // ints used for "for loops". i is the step number,
               // k is the kth vertex for the arrays.
    map<int, Vertex>::iterator vit; // Iterator to traverse through the vertices.
    // Beginning and Ending pointers. (Used for "for" loops)
    map<int, Vertex>::iterator vBegin = Triangulation::vertexTable.begin();
    map<int, Vertex>::iterator vEnd = Triangulation::vertexTable.end();

    double net = 0; // Net and prev hold the current and previous
    double prev;    // net curvatures, repsectively.
    for (k=0; k<p; k++) {
        z[k]=initWeights[k]; // z[k] holds the current weights.
    }
}
```

```

for (i=1; i<numSteps+1; i++)
{ // This is the main loop through each step.
  prev = net; // Set prev to net.
  net = 0;    // Reset net.

  for (k=0, vit = vBegin; k<p && vit != vEnd; k++, vit++)
  {
    // Set the weights of the Triangulation.
    vit->second.setWeight(z[k]);
  }
  if(i == 1) // If first time through, use static method to
  {          // calculate total curvature.
    prev = Triangulation::netCurvature();
  }
  for (k=0, vit = vBegin; k<p && vit != vEnd; k++, vit++)
  { // First "for loop" in whole step calculates everything manually.
    (*weights).push_back( z[k]); // Adds the data to the vector.
    double curv = curvature(vit->second);
    if(curv < 0.00005 && curv > -0.00005)
    { // Adjusted for small numbers. We want it to print nicely.
      (*curvatures).push_back(0.); // Adds the data to the vector.
    }
    else {
      (*curvatures).push_back(curv);
    }
    net += curv; // Calculating the net curvature.
    // Calculates the differential equation, either normalized or
    // standard.
    if(adjF) ta[k]= dt * ((-1) * curv
                        * vit->second.getWeight() +
                        prev / p
                        * vit->second.getWeight());
    else    ta[k] = dt * (-1) * curv
            * vit->second.getWeight();

  }
  for (k=0, vit = vBegin; k<p && vit != vEnd; k++, vit++)
  { // Set the new weights to our triangulation.

```

```

        vit->second.setWeight(z[k]+ta[k]/2);
    }
    for (k=0, vit = vBegin; k<p && vit != vEnd; k++, vit++)
    {
        // Again calculates the differential equation, but we
        // still need the data in ta[] so we use tb[] now.
        if(adjF) tb[k]=dt*adjDiffEQ(vit->first, net);
        else     tb[k]=dt*stdDiffEQ(vit->first);
    }
    for (k=0, vit = vBegin; k<p && vit != vEnd; k++, vit++)
    { // Set the new weights.
        vit->second.setWeight(z[k]+tb[k]/2);
    }
    for (k=0, vit = vBegin; k<p && vit != vEnd; k++, vit++)
    {
        if(adjF) tc[k]=dt*adjDiffEQ(vit->first, net);
        else     tc[k]=dt*stdDiffEQ(vit->first);
    }
    for (k=0, vit = vBegin; k<p && vit != vEnd; k++, vit++)
    { // Set the new weights.
        vit->second.setWeight(z[k]+tc[k]);
    }
    for (k=0, vit = vBegin; k<p && vit != vEnd; k++, vit++)
    {
        if(adjF) td[k]=dt*adjDiffEQ(vit->first, net);
        else     td[k]=dt*stdDiffEQ(vit->first);
    }
    for (k=0; k<p; k++) // Adjust z[k] according to algorithm.
    {
        z[k]=z[k]+(ta[k]+2*tb[k]+2*tc[k]+td[k])/6;
    }
}
}

```

## About the authors

Alex Henniges is a junior double majoring in Math and Computer Science. Thomas Williams is a senior in Comprehensive Mathematics with a minor in Computer Science and a background in Math Education. Mitch Wilson is a senior double majoring in Applied Math and Mechanical Engineering.

Contact information:

- Dr. David Glickenstein- [glickenstein@math.arizona.edu](mailto:glickenstein@math.arizona.edu)
- Alex Henniges- [henniges@email.arizona.edu](mailto:henniges@email.arizona.edu)
- Thomas Williams- [thwillia@email.arizona.edu](mailto:thwillia@email.arizona.edu)
- Mitch Wilson- [mjw@email.arizona.edu](mailto:mjw@email.arizona.edu)